AIAA-2005-3501

FLUIDIC NOZZLE TO IMPROVE TRANSONIC PITCH AND THRUST PERFORMANCE OF HYPERSONIC VEHICLE

Eric J. Gamble*, Rich DeFrancesco†, and Dan Haid‡
SPIRITECH Advanced Products, Inc.
Jupiter, FL, USA

David Buckwalter§
Air Force Research Lab

ABSTRACT

A study has been completed to evaluate the merits of using injection of high-pressure air to control a hypersonic vehicle's pitching moment without adversely impacting the installed nozzle performance. A 3D CFD model was developed and used to investigate the feasibility of using fluidic injection for vehicle control. The underlying critical parameters necessary to control the shock wave location were defined and their effects were quantified. Results have shown that variations in the injection pressure and flow provide changes in the oblique shock angle and that the pressures acting on the SERN ramp are increased in the region of the shock impingement on the ramp. The increase in pressure results in a corresponding change in vehicle moment. However, results have also shown that the resulting performance, when calculated as $CFG_{sec}=F/(Fid_p+Fid_s)$, decreased as flow was injected, providing a net system loss.

The parameters that may be used to control the angle of the oblique shock wave are the pressure, flow, and angle of injection flow. The pressure and flow were independently controlled in the matrix of CFD runs analyzed. The effect of pressure and flow on oblique shock angle are combined in the ideal thrust of the injectant (secondary) flow, which was found to be a critical correlating parameter. Although it is understood that the injection angle is also a critical parameter, its effects were not investigated in detail in this study.

NOMENCLATURE

PT	total pressure
P	static pressure
TT	total temperature
T	static temperature
W	flow
CFG	thrust performance (in terms of primary ideal thrust)
CFGsec	thrust performance (in terms of primary and secondary ideal thrust)
A9	nozzle exit area
A8	nozzle throat area
Fid	ideal thrust
α	injection angle

Subscripts

i	internal
inj	injectant
s	secondary (injectant)
p	primary (main gaspath)
amb	ambient

BACKGROUND

Use of fluidic injection of high-pressure air has been proposed to control a hypersonic vehicle's pitching moment without adversely impacting the installed nozzle performance at off-design, transonic flight conditions. Hypersonic flight vehicles are typically designed with a high expansion ratio Single Expansion Ramp Nozzle (SERN) for a design point at high Mach number flight conditions. However, at low Mach number (transonic) flight, the nozzle is over-expanded, resulting in low, sub-ambient pressures acting on the expansion ramp surface. These sub-ambient pressures cause increased drag, reduced performance, and large pitching moments. The increased drag and corresponding loss in performance may cause as much as 25% loss in net thrust-minus-drag performance throughout much of the transonic flight regime. The corresponding pitching moment is large and must be overcome by increasing the size of the vehicle's control surfaces or

* V.P. New Product Development, SPIRITECH Advanced Products, Inc. , member AIAA
† President, SPIRITECH Advanced Products, Inc., member AIAA
‡ Engineer, SPIRITECH Advanced Products, Inc., member AIAA
§ Project Engineer, AFRL, Wright-Patterson Air Force Base, member AIAA

by shifting the vehicle center-of-gravity. *SPIRITECH*’s “Fluidic Shock Nozzle” was evaluated in this study to determine its ability to decrease transonic drag and pitching moment and improve the overall vehicle performance by injecting high-pressure air into the nozzle to induce a flow separation, thereby increasing the pressures acting on the SERN ramp. This study was focused on demonstrating feasibility of the “Fluidic Shock Nozzle” concept through three-dimensional Computational Fluid Dynamics (3D CFD) analyses.

A representative hypersonic vehicle is shown in Figure 1. As seen in this figure, the aft surface of the vehicle forms an expansion ramp for expanding the exhaust flow to ambient conditions. This ramp is generally sized for the high operating pressures of the ramjet/scramjet at high Mach number conditions. Although SERN nozzles are also considered altitude-compensating nozzles due to the free expansion of the flow along the single expansion ramp, the ramp tends to over-expand the flow to sub-ambient pressures at low nozzle pressure ratios (NPR’s), as shown in Figure 2. This over-expansion is responsible for poor performance and large pitching moments at transonic flight conditions (Figure 3). *SPIRITECH*’s Fluidic Shock Nozzle was designed to use fluidic injection to induce a pressure rise on the SERN ramp (Figure 4), improving performance, and eliminating undesirable pitching moments.

Two separation mechanisms can occur in supersonic nozzles. The first is free shock separation (FSS). This occurs in over-expanded nozzles when the compression required to bring the boundary layer flow at the trailing edge of the nozzle up to ambient conditions induces boundary layer separation. The second is shock-induced separation (SIS). This occurs when a shock impinges on the SERN ramp surface and results in a pressure increase sufficient to separate the flow. *SPIRITECH*’s concept for fluidic injection used in its Fluidic Shock Nozzle employs shock-induced separation to separate the flow from the free expansion surface and create a rise in pressure. This is accomplished by injecting secondary flow from the nozzle cowl trailing edge to generate an oblique shock, which induces a separation on the free expansion surface. The fluidic injection is directed into the primary flow to form a high-pressure region at the trailing edge of the cowl, as shown in Figure 4.

The computational grid for the NASP model 5B is shown in Figure 5. The three-dimensional structured grid contains a symmetry boundary condition through the centerline of the vehicle to help minimize the number of elements. Characteristic boundaries are assumed at the freestream inflows while the nozzle inlet is defined as constant total pressure and temperature. The outflow boundary is set to a constant static pressure. The structured format of the grid allows for sequencing of the grid to accelerate convergence and also helps to identify the required grid size to produce the smallest grid required for acceptable accuracy. The grid is designed to have grid spacing off all viscous walls to provide y+ values of less than one with no grid sequencing. This spacing is lower than the y+ < 3 guideline set by Engblom[1] and resulted in a significantly larger grid size of 14 million cells with no sequencing.

The WIND Version 5.0 solver is a Reynolds Averaged Navier Stokes solver. The default second-order Roe upwind scheme with modification for stretched grids and second-order time marching was used. Mentor’s Shear Stress Transport (SST) turbulence model was used.

The aerodynamic boundary conditions include freestream Mach number and inlet temperature and pressure. The parameters NPR (nozzle pressure ratio) and SPR (secondary pressure ratio) are defined below.

$$NPR = \frac{P_T}{P_{amb}}$$

$$SPR = \frac{Ps_{9i}}{P_{amb}}$$

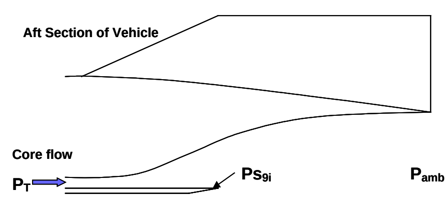

The SPR cannot be set directly; it is a function of the internal expansion ratio and the NPR. The significance of the SPR parameter is that it has the greatest influence on the oblique shock formed at the cowl trailing edge.

Prior to studying the effects of fluidic injection, the CFD model was validated using the test data of Huebner et. al.[2] and the CFD comparisons of Engblom[1]. For this validation study, the Mach 1.2 flight point was selected with a target SPR of 0.486. The results of this CFD compared favorably with data. However, since this validation is not the subject of this study, the details have been omitted from this paper.

INTERNAL INJECTION MODELING

Internal fluidic injection studies were performed to define the relationship between the injection parameters, the resulting oblique shock, and the separation induced by the oblique shock impinging on the SERN ramp. The angle of the oblique shock correlated well with predictions based on the injection pressure and oblique shock theory. Increased static pressure was obtained on the SERN ramp, yielding a change in vehicle moment and an improvement in performance. Further improvement may be possible through more complete separation of the flow along the SERN ramp.

The approach taken in this task was to modify the characteristics of the existing oblique shock formed at the cowl trailing edge in the baseline case. The angle and pressure ratio of the oblique shock in the baseline case is a function of the SPR, as shown by Witte et. al.[2]. The angle and pressure ratio across the oblique shock were seen to increase with decreased SPR (increased backpressure), moving the separation point further upstream. The fluidic injector was located and the parameters set to produce a pressure ratio across the shock greater than that produced at the design SPR.

Design Methodology for Injection

The fluidic injection was located at the trailing edge of the cowl. This point was selected so that the pressure downstream of the shock could be manipulated. The earlier work of Haid and Gamble[3] also suggests that this is the most favorable location to form the separation region that is critical to developing the desired shock.

In addition to injection location, parameters that have been found to control the effectiveness of the fluidic injection include injection flow rate (W_{inj}/W_p), injection pressure (PT_{inj}/PT_P), injection angle (α), the number of injection ports, and the injector geometry (slot, discrete holes, converging port, converging-diverging port). Combinations of these parameters may be used to control the location and angle of the oblique shock. It was beyond the scope of this study to evaluate the effects of this wide range of parameters. Therefore, several assumptions and limits were required:

- With the exception of one configuration, the injection angle (α), defined in Figure 6, was held constant at 45 degrees throughout this study. Although angle variations may have a significant effect on the oblique shock angle, it was decided that the addition of this parameter to the matrix is beyond the scope of this study.

- Options for defining the injector geometry are numerous and include number and location of ports, configuration (slot vs. hole), and exit Mach number (converging vs. converging-diverging hole). For this study, a converging, 2D slot across the width of the cowl was assumed, consistent with prior work by Haid and Gamble[3].

- The range of injection flow rate (W_{inj}/W_P) and injection pressure (PT_{inj}/PT_P) were selected to provide a relative decrease in SPR and corresponding increase in oblique shock angle, as shown in Figure 7.

The theoretical relationship between the oblique shock angle and the static pressure rise across the shock is shown in Figure 7 based on 1D compressible flow theory[4]. The critical flow equations are summarized below. The secondary pressure ratio, SPR, is defined as the ratio of the ideal exit pressure to the backpressure. The ideal exit pressure is a function of the expansion ratio and nozzle pressure ratio while the backpressure is normally equivalent to the ambient pressure. However, in the case of injection, the backpressure is considered to be equal to the static pressure of the injectant flow at the point of injection. The relationship shown in Figure 8 is derived from the independent variables, as summarized below, to provide guidance in selecting the injectant total pressure.

$$SPR = P9_i / PS_{inj}$$

$$PT_{inj} / PS_{inj} = 1.893$$

$$P2 / P1 = PS_{inj} / P9_i$$

$$P9_i / PT_P = f(\gamma, A9_i / A8)$$

Combining this relationship with correlations for predicting flow separation yields the relationship shown in Figure 9. This correlation provided the initial guidance for selecting the injection pressures to be evaluated. (It should be noted that the injection pressure requirements were modified as CFD results became available. The actual pressure rise, as indicated by the CFD results, was considerably less than the theoretical value.)

Injection Matrix and Thrust Calculation

As shown in Table 1, nozzle pressure ratios of 40 and 23 were investigated for a matrix of internal injection configurations. A nozzle pressure ratio of 40 provided a direct comparison with the NASP 5B model data. A nozzle pressure ratio of 23 was selected to provide a secondary pressure ratio, SPR, consistent with a TBCC application. As mentioned previously, the SPR is dependent on both the expansion ratio at the cowl trailing edge and the nozzle pressure ratio. Typical TBCC applications (similar to X-43) use expansion ratios less than those used in the NASP 5B configuration. For the NASP 5B configuration, an SPR consistent with typical TBCC applications was achieved at an NPR of 23. Injectant total pressure ratios (PT_{inj}/PT_P) of 0.1, 0.2, 0.3, and 1.0 were investigated. An injection-to-gaspath total pressure ratio of 1 was selected as the upper limit since it is consistent with the use of fan bypass air to feed the injection slot.

Table 1 - Matrix of CFD Configurations for Internal Injection

INJECTION	CONFIG. #	NPR	PT_{inj}/PT_P	W_{inj}/W_P	Injection Angle
Baseline	2	40	–	0.00	45°
Internal injection	1	40	0.1	0.02	45°
Internal injection	7	40	0.2	0.02	45°
Baseline	3	23	–	0.00	45°
Internal injection	4	23	0.2	0.02	45°
Internal injection	5	23	1.0	0.02	45°
Internal injection	6	23	1.0	0.20	45°
Internal injection	8	23	0.3	0.14	45°
Internal injection	9	23	1.0	0.02	90°

Thrust results were evaluated based on two different definitions for the thrust coefficient. These definitions are summarized:

$$CFG = \frac{\sqrt{Fx^2 + Fy^2}}{Fid_P}$$

$$CFG_{\sec} = \frac{\sqrt{Fx^2 + Fy^2}}{Fid_P + Fid_S}$$

where Fid_P is the ideal thrust of the primary nozzle flow and Fid_S is the ideal thrust of the secondary injectant flow.

Performance calculated in terms of CFG_{sec} provides the most accurate representation of the system-level performance since it accounts for the ideal thrust of both the primary and injectant flows. The injectant flow must be included in the performance calculation since this flow could be used to provide additional thrust if it wasn't injected into the cowl.

Cases 2, 1, and 7 (Table 1), representing a baseline configuration and PT_{inj}/PT_P of 0.1 and 0.2, respectively, were run for the NASP 5B configuration operating at a nozzle pressure ratio of 40. A constant injection flow rate of 2% of W_P was provided in each of these configurations.

Injection Results

As shown in Figure 10, fluidic injection increases the oblique shock angle at the cowl trailing edge, causing the point at which the shock impinges on the SERN ramp to move upstream. Although this produced a net increase in static wall pressure, it did not induce a large-scale separation along the ramp. Figure 11 illustrates that the high injection pressure provided a more uniform static pressure profile, eliminating both the low pressure, over-expansion region and the high pressure, recompression region. The effect on the Mach distribution is illustrated in Figure 12. It is apparent that the high-pressure injection reduces the Mach number, thereby increasing the static pressures.

The associated increase in performance (CFG) is shown in Figure 13. According to this figure, the performance improvement is proportional to the injection pressure, indicating that a high injection pressure may provide the highest thrust improvement. However, as shown in Figure 14, when considering the impact of the injectant ideal thrust, the performance (CFG_{sec}) actually decreases as flow is injected into the nozzle.

Cases 3–6 and 8, representing a baseline configuration and PT_{inj}/PT_P of 0.2, 0.3, and 1.0, were run for the NASP 5B configuration operating at a nozzle pressure ratio of 23. Injection flow areas were sized to provide flow rates of 2-20% for these configurations.

The centerline static pressure distributions for these configurations are shown in Figure 15 while the pressure distribution acting on the SERN ramp surface is summarized in Figure 16. The corresponding Mach contour plots for the different injection configurations are shown in Figure 17. As shown in Figure 15, all injection configurations created an oblique shock and subsequent pressure rise on the SERN ramp.

Internal nozzle performance is shown in Figure 18 and Figure 19 for the configurations evaluated at NPR=23. CFG is shown to increase with increases in PT_{inj}/PT_P for the configurations with high injectant ideal thrust (~20% flow). However, CFG decreases with increases in PT_{inj}/PT_P for configurations with low injectant ideal thrust (2% flow). Comparison of CFG_{sec} for these configurations indicates a performance loss for all injection cases relative to the baseline. In an attempt to improve the performance achieved with injection, the injection angle was increased to 90º (Configuration 9). The performance for this configuration is shown compared to the corresponding configuration with 45º injection (Configuration 5) in Figure 20. As expected, the performance improves as the injection angle increases. The performance for both injection angles is inversely proportional to the injectant-to-primary ideal thrust ratio, as shown in Figure 21. This plot shows that all combinations of injection pressure, flow, and angle provide a loss in performance (CFGsec) relative to the baseline (no injection) case.

The fluidic injection was shown to control the off-axis force acting on the SERN ramp. The projected surface area upon which the vertical force acts is large relative to that for the axial thrust. Therefore, even small changes in the pressure distribution produced by the fluidic injection can cause large changes in the moment acting on the vehicle. This effect could be used to reduce the size requirement for the horizontal control surfaces, thereby reducing overall vehicle drag and weight. Figure 22 illustrates the change in vehicle moment (~12% reduction) that was attained for the internal injection configurations. The normalized vehicle moment, defined in Figure 23, is the moment about the z-axis at the vehicle nose normalized by the moment for the corresponding baseline configuration ($W_{inj}/W_P=0$). The change in moment shows the potential for fluidic injection to be used for vehicle pitch control, reducing the size requirement for horizontal control surfaces.

The ability to use fluidic injection near the trailing edge of the cowl to control the resulting oblique shock angle and the location of its impingement on the SERN ramp was successfully demonstrated in this study. It was shown that variations in the injection pressure and flow provide changes in the oblique shock angle and that the pressures acting on the SERN ramp are increased in the region of the shock impingement on the ramp. The parameters that may be used to control the angle of the oblique shock wave are the pressure, flow, and angle of injection flow. The combined effect of pressure and flow on oblique shock angle is shown by correlating the oblique angle with the ideal thrust of the injectant (secondary) flow, as shown in Figure 24. This figure indicates that large Fid_s is required to produce significant changes to the oblique shock angle. Unfortunately, large Fid_s also results in lower CFG_{sec}.

Prior studies conducted by SPIRITECH using 2D CFD indicated that vehicle moment may be controlled while improving the thrust through use of fluidic injection of secondary flow near the cowl trailing edge. The results of this 3D study, however, showed that the 3D effects are significant and prevent the injection flow from providing an increase in performance, when measured in terms of CFG_{sec}.

Comparison of CFD Results with Theory

The CFD results tended to fall below the separation criteria, indicating that the actual pressure rise across the shock was considerably less than predicted. By correlating the actual pressure rise predicted by the CFD to the theoretical pressure rise expected (Figure 26), a correlation was developed for predicting the injectant pressure required for flow separation. This correlation, updated from that shown in Figure 9 to include the CFD results, is shown in Figure 27. To provide significant flow separation, an injectant total pressure above the curve must be selected.

Oblique Shock Induced by Physical Wedge (No Injection)

According to the equation,

$$CFG_{\sec} = \frac{F_{resultant}}{Fid_P + Fid_S}$$

CFG_{sec} may be improved either by reducing the ideal thrust of the injectant (secondary) flow or by increasing the resulting thrust (while holding Fid_s constant). Up to this point, CFD studies have focused on increasing the resultant thrust ($F_{resultant}$), even though they resulted in increases to the injectant ideal thrust (Fid_s). To achieve the objective of eliminating the ideal thrust of the injectant flow from the equation, an analysis was conducted of a configuration that used a physical wedge rather than injection flow to create an oblique shock. It was suggested that a wedge positioned at the point of fluidic injection on the lower cowl could be sized to produce the same effect on the upper SERN as the injection. If $F_{resultant}$ can be held constant while decreasing Fid_s, then a net improvement in CFG_{sec} will result.

To correctly size the wedge, the measured oblique shock angles (derived from the CFD results) and the effective blockage at the exit of the internal portion of the nozzle were determined, as summarized in Table 2. The indicated point (PT_S/PT_P=0.2, W_S/W_P=0.02) was selected for this study. The wedge geometry was defined based on a 35.5º wedge angle and 6.7% blockage at $A9_i$.

Table 2 - Physical Sizing of Wedge Angle

NPR	PTS/PTP	WS/WP	CFD Measured SHOCK ANGLE	WEDGE ANGLE	$A9_{int}$ BLOCKAGE
23	.2	.02	57	35.5	6.7%
23	1	.17	90	34	14.5%
23	1	.02	44	28.5	2%
40	.1	.02	37	23.5	4.6%
40	.2	.02	53	33.5	6.7%

As shown in Figure 28, the wedge produced an oblique shock. However, the shock was only slightly stronger than that observed in the baseline configuration (without injection). It did not produce the expected 57º oblique shock that was observed in the injection configuration that it attempted to simulate. A normalized moment of 0.993 was achieved, which was much less than the 1.040 normalized moment achieved by the comparable fluidic injection configuration. Although the shock was not as strong as anticipated, a net improvement in CFG_{sec} of nearly 1% was measured. These results indicate that an increased wedge angle may be worth investigating for improving performance. However, it should be noted that the increase in performance may be caused by a reduction in $A9_i$ rather than a result of the slight increase in SERN pressures. Since the nozzle is considerably over-expanded for this off-design configuration, any reduction in $A9_i$ could result in significant thrust improvement.

CONCLUSIONS

The ability to use fluidic injection near the trailing edge of the cowl to control the resulting oblique shock angle and the location of its impingement on the SERN ramp was successfully demonstrated in this study. It was shown that variations in the injection pressure and flow provide changes in the oblique shock angle and that the pressures acting on the SERN ramp are increased in the region of the shock impingement on the ramp. The increased pressures acting on the SERN ramp induce a moment on the vehicle, allowing for attitude control. However, it was also found that the resulting performance, when calculated as $CFG_{sec}=F/(Fid_p+Fid_s)$, decreased as flow was injected. Prior studies conducted by *SPIRITECH* using 2D CFD indicated that the thrust of a hypersonic vehicle operating at transonic conditions is improved through use of fluidic injection of secondary flow near the cowl trailing edge. The results of this 3D study, however, showed that the 3D effects are significant and prevent the injection flow from providing an increase in performance, when measured in terms of CFG_{sec}.

The parameters that may be used to control the angle of the oblique shock wave are the pressure, flow, and angle of the injection flow. The pressure and flow were independently controlled in the matrix of CFD runs analyzed. The effect of pressure and flow on oblique shock angle are combined in the ideal thrust of the injectant (secondary) flow, which was found to be a critical correlating parameter. Although it is understood that the injection angle is also a critical parameter, its effects were not investigated in detail in this study.

Incorporation of a physical wedge rather than fluidic injection to induce an oblique shock provided the most significant increase in thrust (~1%). Although this thrust improvement may be the result of a reduction in the nozzle exit area, further studies based on non-fluidic methods may provide additional thrust improvements.

REFERENCES

[1] W.A. Engblom, “Numerical Prediction of SERN Performance Using WIND Code”, AIAA-2003-4410

[2] Lawrence D. Huebner, David W. Witte, Earl H. Andrews, Jr., “Exhaust Simulation Testing of a Hypersonic Airbreathing Model at Transonic Speeds”, AIAA-2003-7001

[3] D.A. Haid, E.J. Gamble, “Improving Off-Design Nozzle Performance Using Fluidic Injection”, AIAA-2004-1206, January 2004

[4] NACA Report 1135

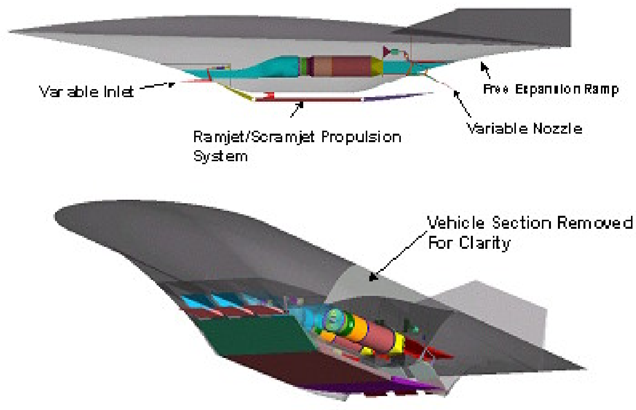

Figure 1 - Hypersonic Propulsion / Vehicle Integration

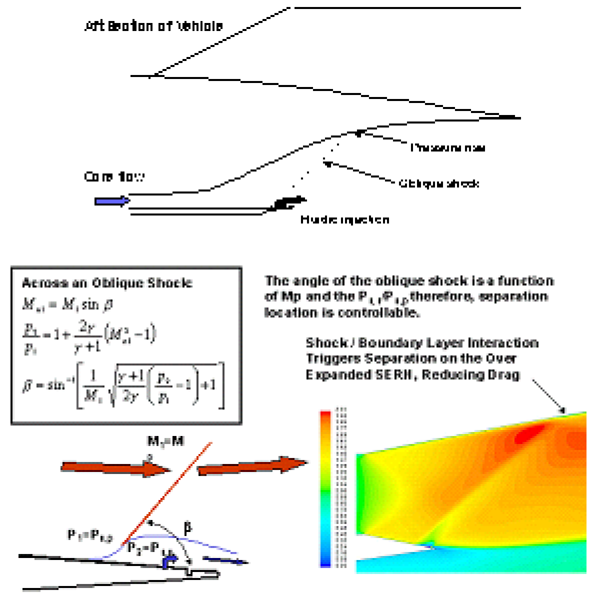

Figure 4 - Oblique Shock Produces Static Pressure Rise

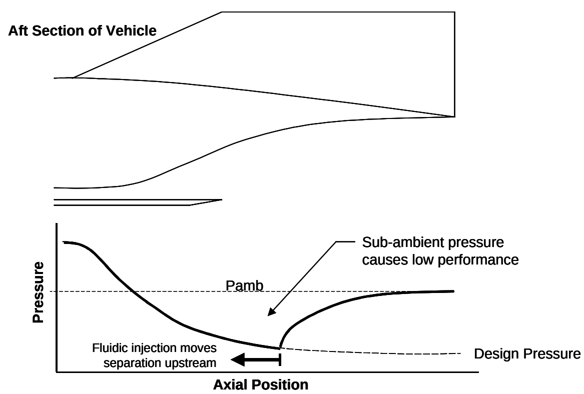

Figure 2 - Sub-Ambient Pressures Exist on SERN Ramp

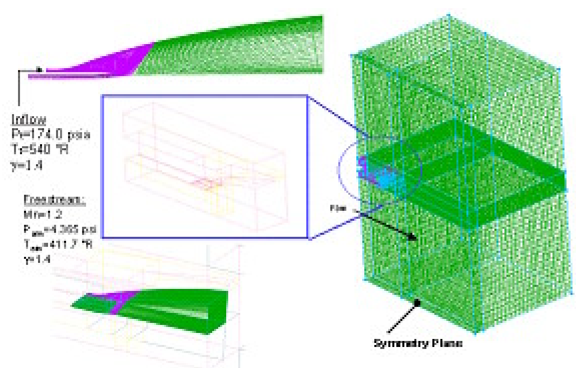

Figure 5 – CFD Mesh and Boundary Conditions

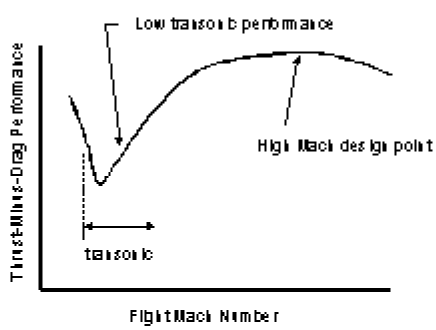

Figure 3 - Typical Thrust-Minus-Drag Performance

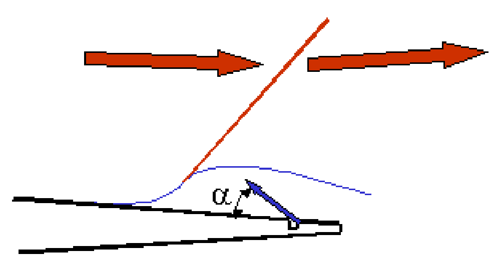

Figure 6 - Injection Angle Definition

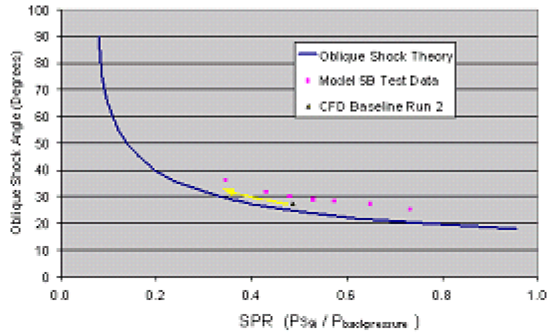

Figure 7 - Oblique Shock Angle as a Function of Static Pressure Rise Across the Shock

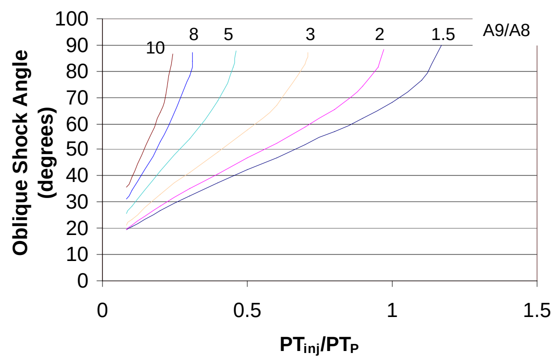

Figure 8 - Oblique Shock Angle as a Function of Injection Total Pressure

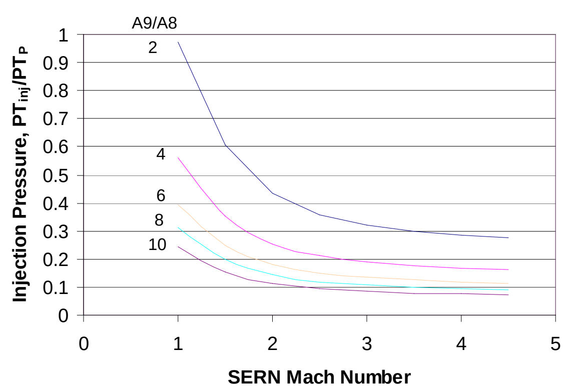

Figure 9 - Injection Total Pressure Criteria for SERN Separation

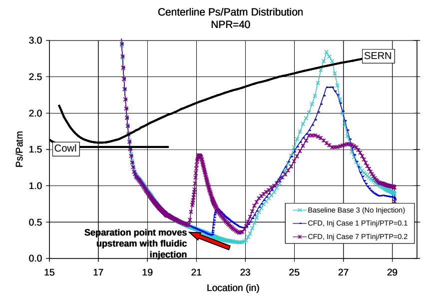

Figure 10 - Effect of Injection Pressure on SERN Centerline Pressures for Baseline Configuration (NPR=40)

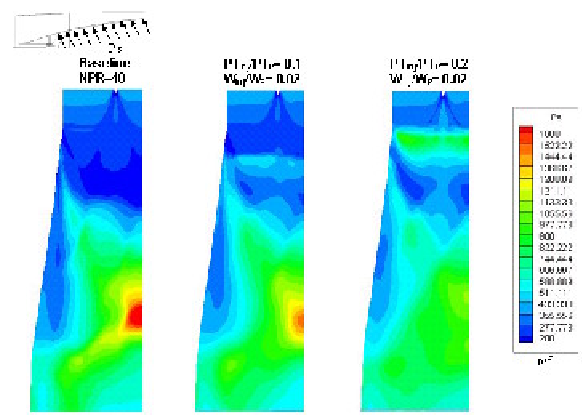

Figure 11 - Effect of Injection Pressure on SERN Ramp Static Pressure Distribution (NPR=40)

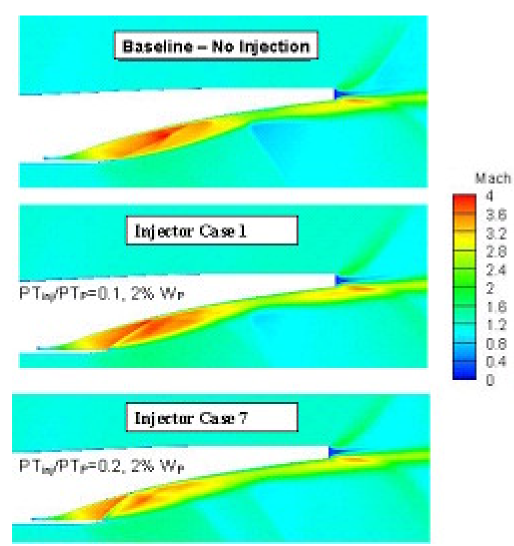

Figure 12 - Effect of Injection Pressure on Centerline Mach Contours (NPR=40)

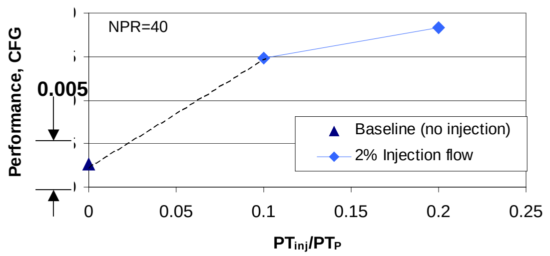

Figure 13 - Effect of Injection Pressure on CFG Performance for NPR=40 (W_{inj}/W_8=2%)

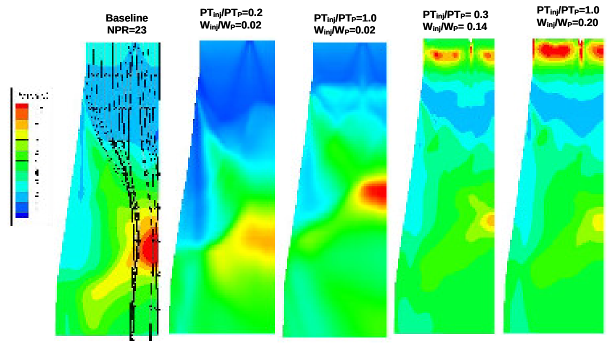

Figure 16 - Effect of Injection Pressure on SERN Ramp Static Pressure Distribution (NPR=23)

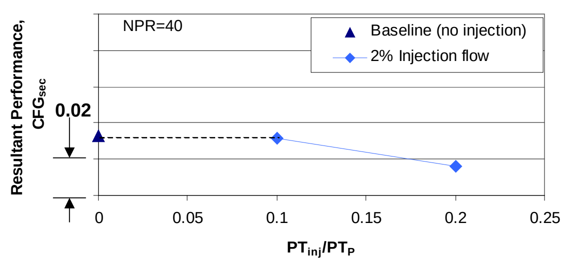

Figure 14 - Effect of Injection Pressure on CFG_{sec} Performance for NPR=40 (W_{inj}/W_8=2%)

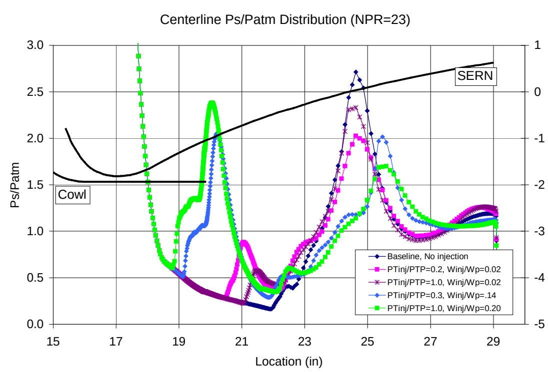

Figure 15 – Centerline SERN Static Pressure Distribution for Injection at NPR=23

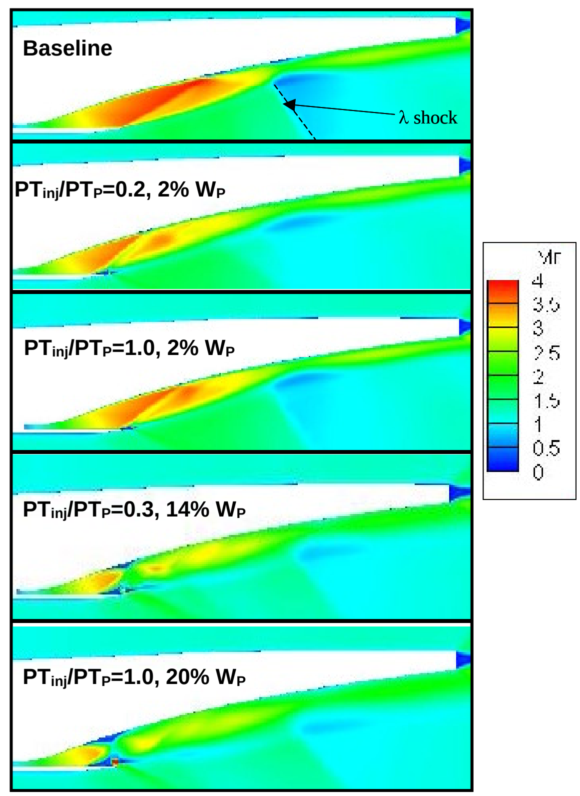

Figure 17 – Effect of Injection Pressure on Centerline Mach Contours (NPR=23)

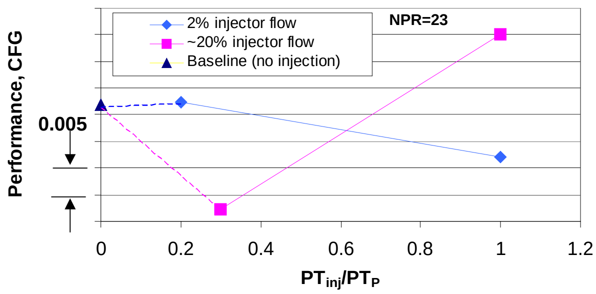

Figure 18 - Effect of Injection Total Pressure on Nozzle Performance, CFG (NPR=23)

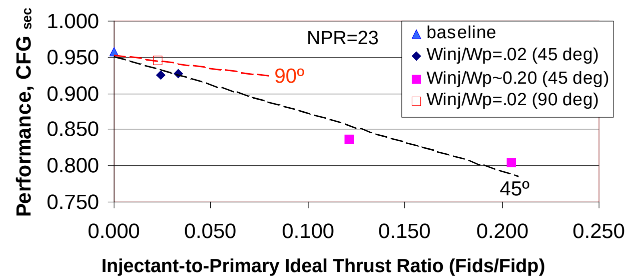

Figure 21 - Performance (CFGsec) Correlated with Ideal Thrust Ratio

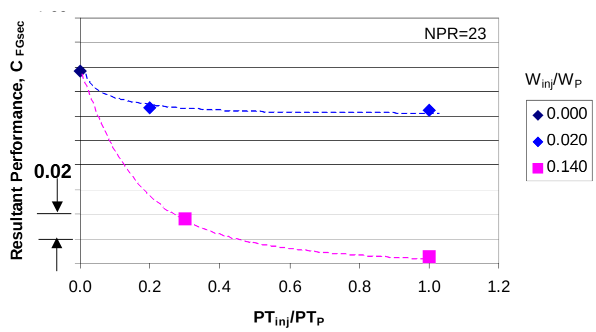

Figure 19 - Effect of Injection Total Pressure on Nozzle Performance, CFG_{sec} (NPR=23)

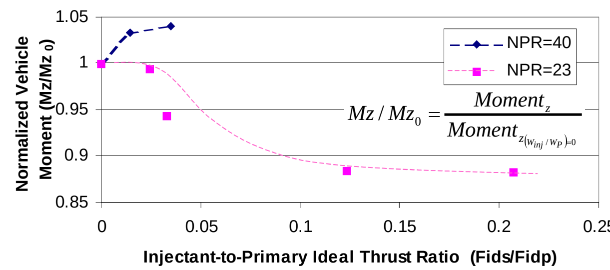

Figure 22 - Normalized Vehicle Moment Correlated with Ideal Thrust Ratio

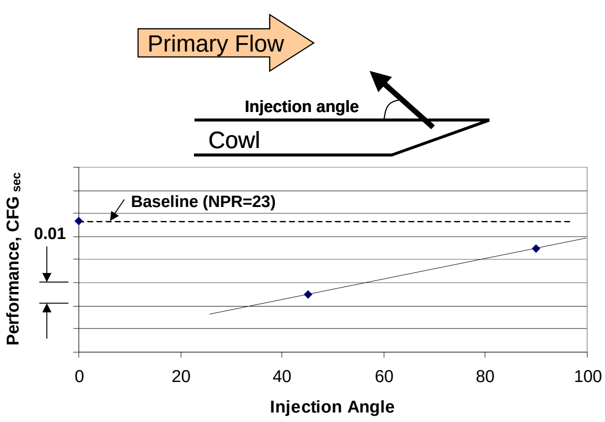

Figure 20 - Effect of Injection Angle on Performance, CFGsec

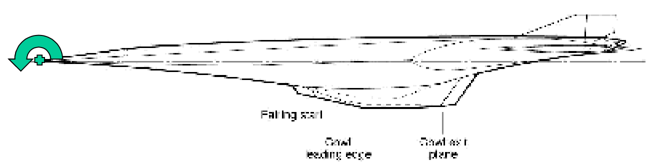

Figure 23 - Vehicle Moment Definition

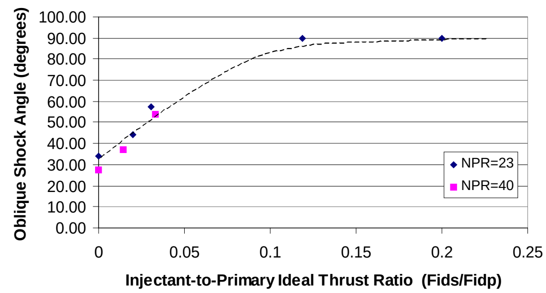

Figure 24 - Oblique Shock Angle as Function of Ideal Thrust Ratio

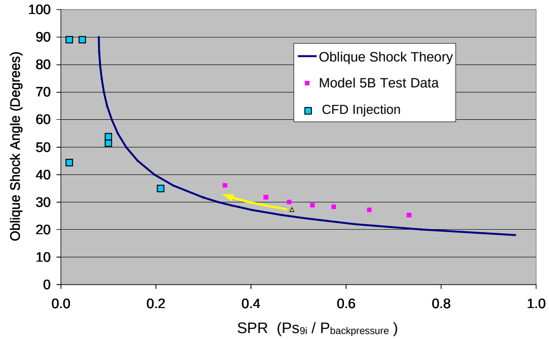

Figure 25 - Oblique Shock Angle as a Function of Static Pressure Rise Across the Shock

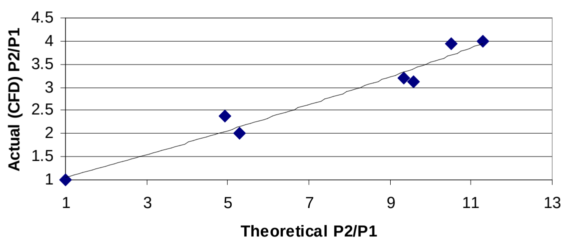

Figure 26 - Relationship Between Actual and Theoretical Static Pressure Rise Across Oblique Shock

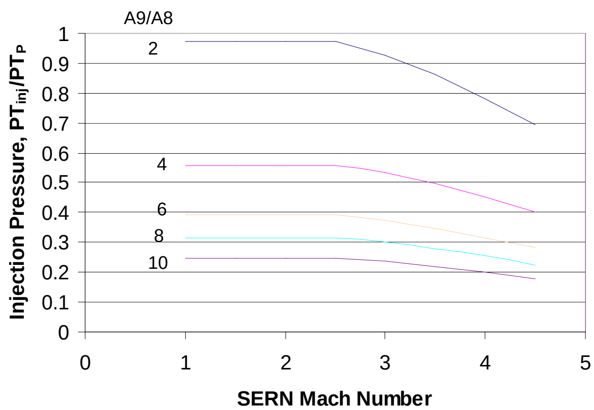

Figure 27 - Injection Total Pressure Criteria for SERN Separation, Based on CFD Results

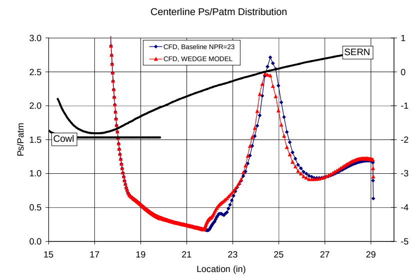

Configuration	Measured Shock Angle	ΔCFG_{sec}
Baseline	34.1	0
PTS/PTP=0.2 WS/WP=0.02	57.3	-0.030
Wedge	**35.6**	**0.008**

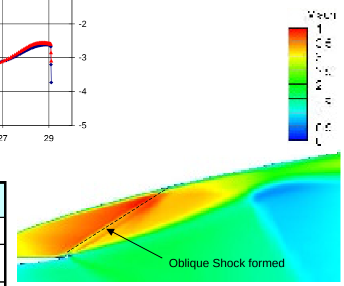

Figure 28 - CFD Results for Physical Wedge (No Injection)